Physically Based Boiling Simulation with Thermally Driven Dynamic Nucleation

PENG PENG YE YONGLONG
Digital ART Laboratory of Shanghai Jiao Tong University
Shanghai Jiao Tong University, Shanghai, 200240, Shanghai, China
pengpengye@sjtu.edu.cn

Xubo Yang
Digital ART Laboratory of Shanghai Jiao Tong University
Shanghai Jiao Tong University, Shanghai, 200240, Shanghai, China
yangxubo@sjtu.edu.cn

Abstract

Boiling is a complex physical phenomenon with extensive applications in both natural and engineering systems. In this work, we develop a particle-based simulation method that models the boiling process, reproduces the superheating phenomenon, and includes an associated treatment mechanism. "Superheated" is a metastable state and accurate modeling of superheated liquids is critical in boiling simulations. To maintain thermal stability and avoid excessive energy accumulation in superheated liquid regions, we introduce a thermally driven dynamic nucleation mechanism to model localized explosive boiling. Phase transitions are fundamental mechanisms underlying boiling phenomena. A phase transition requires both thermodynamic and kinetic conditions: the system must reach a critical temperature, and nucleation sites or disturbances must be present to reduce the energy barrier for liquid–vapor transition, whereas previous simulation approaches have often focused primarily on the thermodynamic condition and paid limited attention to kinetic condition. Moreover, heat conduction and convection induce complex liquid behaviors that may interrupt or resume the phase transition. To address these challenges, we have developed a novel energy transfer mechanism for phase transitions. Finally, the connected vapor particles were identified and regarded as individual bubbles. An bubble oscillation constraint was introduced to simulate the periodic expansion and contraction of bubbles, thereby enhancing the realism of bubble rising behavior.

Keywords: ***Boiling simulation, Bubble simulation, Position-based fluids, Phase transition modeling, Thermal dynamics, Superheated Liquid***

1. Introduction

Physical simulations are a popular research area in computer graphics. Over the past few decades, many researchers have studied topics such as cloth, fluid, and hair simulation, delivering visually compelling results by combining accurate modeling with realistic rendering. Boiling simulations are challenging problems within the field of fluid simulations due to their complex multiphase and thermodynamic phenomena. Fluid simulation methods can be broadly classified into Eulerian and Lagrangian approaches. As noted by Li et al.[12] , Eulerian methods often struggle to accurately capture free surfaces and gas–liquid interfaces, especially in phenomena involving continuous topological changes such as boiling. In contrast, Lagrangian methods can precisely track moving boundaries and significantly simplify the solution of governing equations. Among Lagrangian approaches, Smoothed Particle Hydrodynamics (SPH) has been widely used for fluid simulation due to its physically grounded formulation. However, SPH often suffers from numerical instability near free surfaces, where particle deficiency can cause density errors and pressure oscillations. Moreover, it requires small time steps to maintain stability, limiting its efficiency in large-scale or interactive simulations.

To address these limitations, we adopt the Position-Based Fluids (PBF) framework [15], which integrates incompressibility constraints into the Position-Based Dynamics (PBD) model [18]. Instead of explicitly computing forces, PBF iteratively corrects particle positions through constraint projection, achieving robust and stable results even with large time steps. Building upon this framework, our method further incorporates thermal energy transfer and dynamic nucleation models to handle phase-change phenomena in boiling.

As is well known, during actual boiling, bubbles are often surrounded by a layer of superheated liquid. Stojanovi

[21] noted that 83% of the heat transfer to bubbles originates from this surrounding superheated liquid layer. Superheating is a common phenomenon in boiling. Moreover, boiling involves phase transition phenomena that require the simultaneous fulfillment of a thermodynamic condition, that a critical temperature is reached, and a kinetic condition, that nucleation sites or perturbations are present to reduce the energy barrier for the liquid-to-vapor transition. Previous studies primarily focused on thermodynamic conditions while overlooking the kinetic constraints of phase transition, and therefore did not sufficiently model the superheated liquid state or its associated metastable behavior. Most previously established particle-based boiling simulation methods [8][12] first establish a heat conduction system based on Fourier's law and then generate bubbles according to the predefined nucleation sites. However, in boiling simulations, these methods ignore the kinetic condition of phase transition. In the method of Gu et al.[8], a particle enters the latent-heat accumulation stage as soon as it satisfies the thermodynamic condition, meaning that superheating cannot be reproduced. In the approach of Li et al.[12], phase transition is restricted to predefined nucleation sites, without properly evaluating either the thermodynamic or kinetic conditions of the surrounding liquid particles. Prakash [19] noted that nucleation sites near superheated liquid regions are activated to generate bubbles. However, this approach does not fully comply with the law of conservation of energy and is restricted to activating predefined nucleation sites, thereby failing to address situations where superheated liquid lacks nearby nucleation sites.

Superheating is a metastable state that can compromise system stability and, in practice, may lead to explosive boiling. During this process, a large volume of superheated liquid rapidly undergoes a phase transition, bringing the local temperature back to equilibrium. According to Classical Nucleation Theory, as superheating intensifies, local energy fluctuations can induce internal cavities or perturbations, initiating explosive boiling. Building on this insight, we introduce a thermally driven dynamic nucleation method. When the local energy exceeds a critical threshold, transient internal cavities are assumed to emerge, serving as short-lived nucleation sites. This allows the superheated liquid to fulfill the kinetic conditions for a phase transition, converting the superheated portion of sensible heat into latent heat and restoring thermal stability.

Thermal energy can be divided into two categories: sensible heatand latent heat. Sensible heat is directly related to temperature changes and is essential for modeling heat conduction and convection processes. In contrast, latent heat refers to the energy absorbed or released in the course of a phase transition. Owing to the coupled effects of the phase transition, heat conduction, and convection, the liquid exhibits a variety of complex behaviors. For instance, during the latent heat accumulation phase, nucleation sites may become deactivated or be advected away by convective currents, leading to an interruption of the phase transition. In contrast, superheated particles migrating toward a nucleation site may restore the phase transition process. These dynamics involve continuous exchange and storage of both sensible heat and latent heat. Traditional heat transfer models are inadequate for capturing the complexities of boiling, as phase transition conditions are influenced by both thermodynamic and kinetic factors. Under the influence of convective heat transfer, particles can induce rapid changes in the phase transition conditions, requiring corresponding adjustments in the handling of the sensible and latent heat. We have developed a comprehensive energy transfer mechanism for phase transitions, differentiating between the sensible and latent heat processes. Additionally, based on the satisfaction of thermodynamic and kinetic conditions, we classify particles into several states: normal liquid, undergoing a phase transition, superheated liquid, and vapor. When particles undergo state transitions driven by phase transition conditions, the corresponding sensible and latent heat treatments are applied to comply with the law of conservation of energy and ensure accurate particle behavior.

We performed a connectivity analysis on vapor particles, identifying each connected group as an individual bubble. Based on our experimental observations, we then designed an empirical bubble oscillation constraint that enables the bubbles to undergo periodic expansion and contraction. This constraint reproduces the oscillatory behavior commonly observed in real boiling, resulting in more realistic bubble rising effects.

In summary, the main contributions of this paper are as follows:

1. A thermally driven dynamic nucleation model is developed that not only simulates superheating but also resolves it through the dynamic creation of nucleation sites.

2. A dual-channel phase transition model is established using a multi-state particle system to dynamically switch between sensible and latent heat while ensuring energy conservation.

3. An empirical bubble oscillation constraint is introduced to simulate the periodic expansion and contraction of bubbles, enhancing the realism of bubble rising behaviors.

2. Related Work

2.1. Fluid simulation

Fluid simulation has long been a core research area in computer graphics. The SPH, initially developed for astrophysical simulations[14], was later adapted for fluid modeling [17]. As a Lagrangian particle-based approach, SPH inherently manages free surfaces and complex topological

variations, making it suitable for multiphase and boiling simulations. Subsequent studies have focused on enhancing its performance and incompressibility, resulting in several improved variants, such as predictive-corrective SPH [20], implicit incompressible SPH [9], and divergence-free SPH [1]. In 2007, Müller et al. introduced the PBD method [18], which provides a unified framework for simulating deformable objects by directly enforcing geometric constraints on particle positions. Unlike conventional force-based approaches, such as SPH, PBD resolves dynamics through iterative position corrections, ensuring unconditional stability even under large time steps. Since then, the PBD method has been widely used in scenarios dealing with collisions and constraints due to its advantage of direct manipulation of the particle positions. Subsequently, in 2013, Müller et al. proposed the PBF method [15]. The PBF method extends the PBD method for fluid simulations by incorporating an iterative density solver that enforces incompressibility constraints on Lagrangian particles, thereby directly correcting their positions. Since it was proposed, the PBF method has been widely adopted in fluid simulations due to its excellent results.

2.2. Boiling simulations

Boiling simulations have been a significant topic in fluid simulations. In 2006, Mihalef et al. [16] proposed an Eulerian boiling simulation method that seeds bubbles at nucleation sites with an arbitrary frequency. Kim and Carlson [11] extended the Yanagita model by treating boiling as a separate computational module. Bulbul et al. [2] used a simple real-time particle system to simulate the boiling phenomenon, modeling bubbles and wavicles as particles while using a grid method to handle heating and fluid surfaces. When the floor grid reached 100°C, a bubble was generated at a random position within the grid. Prakash et al. [19] introduced a discrete-particle-based method to simulate the entire boiling process using the SPH method. They established multiple nucleation sites, which switched from an inactive to an active state and produced bubbles when conditions were met. Gu et al. [8] modeled the boiling phenomenon in phases and proposed a vapor bubble model for bubble condensation and merging. They pretreated certain water particles to move them toward nucleation sites, where they would convert into bubbles once the temperature reached 100°C and the absorbed heat exceeded a threshold. Li and Xiao [12] proposed a boiling simulation framework based on the PBF method, incorporating a simplified mass transfer model and a more refined heat transfer model, where water particles near the nucleation site transferred mass and heat, generating bubbles when the vapor mass at the nucleation point reached a threshold. Chen [4] introduced a new method to simulate boiling without bubbles, capturing the splashing effect of intense boiling. However, previous methods largely neglect the superheated liquid state and lack mechanisms to address its metastable behavior. Gu et al. [8] enforced only the thermodynamic condition for phase change while ignoring the kinetic requirement, thereby preventing the formation of superheated liquid and excluding superheating phenomena from their simulations. Similarly, Li and Xiao [12] omitted the kinetic condition and limited phase change to predefined nucleation sites, permitting only a single bubble to form at each site at a time. In contrast, the proposed method, developed within the PBF framework, explicitly incorporated both thermodynamic and kinetic conditions, modeled superheating, and introduced a dynamic nucleation mechanism that allowed multiple simultaneous phase transitions. A concise comparison is summarized in Table 1.

2.3. Phase transitions

Modeling melting and solidification through heat transfer has long been a key topic in computer graphics. Stora et al.[23] first introduced a physics-based fluid-to-solid transition for simulating magma, providing an early framework for phase change modeling. Carlson et al.[3] extended this idea by treating solids as high-viscosity fluids and coupling heat diffusion with state changes, improving the realism of melting processes. Subsequent works enhanced interface and material modeling: Iwasaki et al.[10] incorporated surface tension to capture droplet dynamics, Clausen et al.[5] used FEM to unify fluid, elastic, and plastic behaviors, and Stomakhin et al.[22] applied MPM with dynamic material properties for large-scale simulations, later accelerated by Gao et al.[7]. Ding et al.[6] modeled thermo-mechanical coupling in food materials, while Su et al.[24] and Tu et al.[25] developed viscoelastic liquid phase change frameworks with improved thermodynamic consistency and computational efficiency. Recent applications include thin film freezing and complex interface phenomena using MELP[13]. These works collectively advanced the physical accuracy, numerical stability, and visual realism of phase change simulations across materials and scenarios.

3. Boiling Simulation

3.1. Position-based fluids (PBF) method

In the PBF method [15], each particle is associated with a density constraint, which is expressed as a function of its own position and the positions of its neighbors, collectively denoted as $\mathbf{p_1}$,...,$\mathbf{p_n}$. The density constraint on particle i is defined using an equation of state:

$$C_i\left(\mathbf{p}_1, \ldots, \mathbf{p}_n\right) = \frac{\rho_i}{\rho_0} - 1, \tag{1}$$

Table 1: Comparison of overall methods and modeling approaches.

	Method	Superheat Capability	Phase Transition Condition	Phase-Transition Candidate Particle	Superheat Treatment
Gu et al.	SPH	No	Thermodynamic only	Liquid particles	No
Li and Xiao	PBF	Yes	Thermodynamic only	Preset nucleation sites	No
Ours	**PBF**	**Yes**	**Thermodynamic + Kinetic**	**Liquid particles**	**Yes**

where ρ_0 is the rest density, and the expression for ρ_i is

$$\rho_i = \sum_{j \in \mathcal{N}(i)} m_j W\left(\mathbf{p}_i - \mathbf{p}_j, h\right), \tag{2}$$

where m_j denotes the mass of the neighboring particle j of particle i, $N(i)$ is the set of neighboring particles of particle i, and W is a smoothing kernel function.

The primary role of the density constraint equation is to enforce incompressibility. To satisfy the density constraint, the PBF method systematically computes position corrections for each particle based on the gradients of the constraints and Lagrange multipliers, and it iteratively updates the particle positions until the density at each particle converges to the target value ρ_0. This systematic correction prevents the fluid from being overly compressed or expanded, thereby maintaining physically realistic fluid behavior.

3.2. Nucleation sites

Our method models two types of nucleation: preset nucleation sites that represent fixed cavities on the surface, and dynamic nucleation sites that emerge spontaneously in superheated regions. Preset nucleation sites are long-lasting and spatially fixed, representing microcavities on container walls. These sites provide the necessary kinetic conditions for phase transition in boiling simulations, ensuring proper bubble formation. Without them, normal phase transition cannot occur. By attracting nearby liquid particles, they promote higher local heat flux and enhance overall heat transfer. Based on Classical Nucleation Theory, they serve as favorable locations for heterogeneous nucleation. In contrast, dynamic nucleation refers to a transient phenomenon in which a superheated liquid continuously absorbs heat until local energy fluctuations trigger the spontaneous formation of internal voids or perturbations. These nascent cavities act as nucleation sites, facilitating the rapid release of excess thermal energy from the surrounding superheated liquid, thus restoring local thermal equilibrium. As such, dynamic nucleation acts as a critical safeguard mechanism for modeling the superheated metastable state in boiling.

3.2.1 Preset nucleation sites

The bottom surface was divided into several fixed regions, where preset nucleation sites were placed at predetermined positions on the container base. To evaluate the influence of the number of preset nucleation sites on superheating behavior, we conducted a series of experiments with different nucleation site counts and measured the evolution of superheated particles, as shown in Figure 1. The results indicate that, as time progresses, the number of superheated particles in all experimental groups gradually converges to a similar stable level. This suggests that the preset nucleation site count has a limited impact on the overall superheating phenomenon. Instead, it primarily affects the rate of bubble generation and heat transfer, since these preset sites attract nearby liquid particles that carry higher heat flux during thermal exchange.

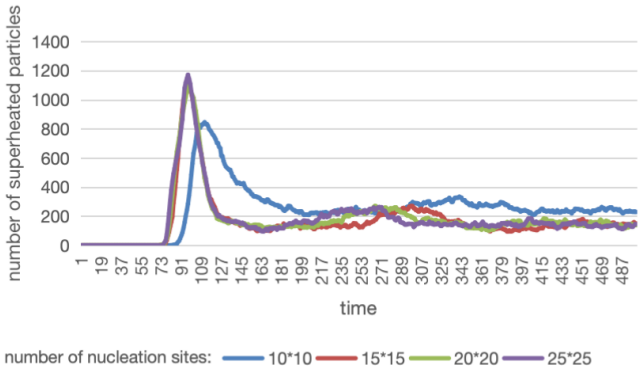

Figure 1: Time evolution diagram of superheated particles with varying numbers of preset nucleation sites.

3.2.2 Dynamic nucleation

The superheated state is a metastable condition in which the liquid temperature has reached the saturation point but no vapor nucleation sites are present nearby. To prevent such superheating from destabilizing the system, we propose a dynamic nucleation method. When the local thermal energy of a superheated liquid exceeds a critical threshold, an internal cavity is assumed to form, representing the transient emergence of a new nucleation site. This process triggers localized explosive boiling, allowing the excess thermal energy to be rapidly released and the system to return to a stable state. The detailed implementation is described below. In reality, during the phase transition of a liquid, the sensible heat Q_{sens} stored in the liquid region can be expressed as:

$$Q_{sens} = mc\left(T - T_{\text{sat}}\right), \tag{3}$$

where m is the liquid mass, c is the specific heat capacity, T is the instantaneous liquid temperature, and T_{sat} is the saturation temperature.

Water requires a substantial amount of energy to evaporate, referred to as the latent heat of vaporization ($L = 2.26 \times 10^6$ J/kg). The mass of liquid evaporation P is defined as follows:

$$P = Q_{sens}/L. \tag{4}$$

That is, for every m kg of liquid, P kg will evaporate.

Accordingly, each superheated liquid particle is considered the center of a local liquid region encompassing itself and its neighbors. The total excess sensible heat stored in this region is calculated as the sum of the sensible heat of superheated particle i and its superheated neighboring liquid particles, expressed as:

$$Q_{sens} = \sum_{i \in k} m_i c \left(T_i - T_{\text{sat}}\right), \tag{5}$$

where k denotes the set of superheated particles among the neighbors of superheated particle i. Dynamic nucleation is triggered only when the accumulated excess sensible heat exceeds a critical threshold. Following empirical testing, we set this threshold to $Q_{\text{crit}} = 10 m_p L$, where m_p is the mass of a liquid particle. The stored total excess sensible heat results in the phase transition of n liquid particles to the vapor state:

$$n = \lfloor Q_{sens}/L \rfloor. \tag{6}$$

We employ the Fisher–Yates shuffle algorithm to generate a uniformly random permutation of all candidate particles, ensuring that each particle has an equal probability of being selected without repetition. After shuffling, the first n particles are chosen to undergo a phase transition. The associated residual energy is then expressed as

$$Q_{residual} = Q_{sens} - n \cdot L, \tag{7}$$

$Q_{residual}$ will be converted back to sensible heat and evenly distributed among the remaining $k - n$ liquid particles.

Through this process, localized energy excess leads to the formation of internal cavities, triggering a phase transition in the superheated liquid. This converts the superheated portion of the sensible heat into latent heat, thereby restoring the liquid's energy to a stable state. This process ensures energy conservation and can handle complex scenarios such as interruptions and resumptions of phase transitions. The detailed implementation is described in Section 3.3.2.

3.3. Energy transfer system

A very important element of the boiling phenomenon is the phase change, and a boiling simulation is incomplete without it. The realization of the phase transition involves thermal dynamics, including heat conduction and convection. Thus, a complete energy transfer mechanism is crucial for simulating boiling.

When liquid particles meet the thermodynamic and kinetic conditions, they will enter an energy storage phase. During this stage, the absorbed sensible heat is converted into latent heat. Once the latent heat reaches a threshold, the particles accumulate sufficient energy to overcome the liquid–vapor phase barrier and transition to the vapor phase. In the following sections, we will discuss thermodynamics and the handling of phase transitions.

3.3.1 Thermodynamics

There are three primary modes of heat transfer: conduction, convection, and radiation. Conduction occurs when heat is transferred through direct contact between objects at different temperatures. Convection arises when temperature differences within a fluid lead to density variations, causing the fluid to circulate and transfer heat through the movement of its particles. Heat radiation is electromagnetic radiation emitted due to the thermal motion of particles within a material. However, it is typically neglected in boiling simulations because its contribution is minor compared to conduction and convection. In the absence of phase transitions, the heat conducted and convected by particles is classified as sensible heat.

Heat transfer occurs due to the temperature difference between two objects, causing thermal energy to move from the hotter object to the cooler one. During boiling, thermal energy exchange primarily occurs in two ways: heat conduction between the heat source and the particles, and heat conduction between the particles themselves. The heat conduction is controlled by Fourier's law:

$$\mathbf{q} = -k \nabla T, \tag{8}$$

where $\mathbf{q}$ is the heat flux, k is the thermal conductivity, and ∇T is the temperature gradient. The total internal energy in a control volume V is

$$E = \int_V Q_v dV, \tag{9}$$

where Q_v is the thermal energy density per unit volume. According to conservation of energy,

$$\frac{d}{dt} \int_V Q_v dV = - \oint_{\partial V} \mathbf{q} \cdot \mathbf{n} dS + \int_V q_s dV, \tag{10}$$

where $\mathbf{q}$ is the heat flux vector, $\mathbf{n}$ is the outward normal of the boundary surface ∂V, and q_s is the heat acquired per unit volume from the heat source. We use the divergence theorem to convert the surface integral to a volume integral:

$$\oint_{\partial V} \mathbf{q} \cdot \mathbf{n} ds = \int_V \nabla \cdot \mathbf{q} dV. \tag{11}$$

Substituting this into equation (10), we obtain

$$\frac{d}{dt}\int_V Q_v dv = -\int_V \nabla \cdot \mathbf{q} dV + \int_V q_S dV. \tag{12}$$

According to the Leibniz integral rule, we obtain

$$\frac{d}{dt}\int_V Q_v dv = \int_V \frac{\partial Q_v}{\partial t} dv. \tag{13}$$

Substituting this into equation (12), we obtain

$$\int_V \frac{\partial Q_v}{\partial t} dv = -\int_V \nabla \cdot \mathbf{q} dV + \int_V q_S dV. \tag{14}$$

By eliminating the integral, we obtain the local form:

$$\frac{\partial Q_v}{\partial t} = -\nabla \cdot \mathbf{q} + q_s. \tag{15}$$

Substituting in equation (8) yields

$$\frac{\partial Q_v}{\partial t} = k\nabla^2 T + q_s. \tag{16}$$

According to Gu [8], the Laplacian operator is

$$\nabla^2 T_i = \sum_{j=1}^{n} \frac{m_j}{\rho_j} \frac{4\rho_i}{\rho_i + \rho_j} \frac{\mathbf{p_{ij}} \left(T_i - T_j\right)}{\mathbf{p_{ij}}^2 + 0.01h^2} \nabla W\left(\mathbf{p_{ij}}, h\right), \tag{17}$$

where n is the number of neighbors of particle i, m_j is the masses of particle j, respectively, ρ_i and ρ_j represent the density of particle i and j, and $\mathbf{p_{ij}}$ is a vector expressing the relative positions of particles i and j.

Heat convection also plays a crucial role in boiling dynamics. Following the approach of Gu et al. [8], we model convective motion by considering the temperature distribution among liquid particles. Specifically, particles in lower regions generally possess higher temperatures, creating an upward thermal gradient that drives the fluid motion. For each liquid particle, we compute the cumulative temperature gradient vector to estimate the preferred rising direction. Particles following this direction transport thermal energy upward, which is subsequently redistributed to neighboring cooler particles through conduction.

3.3.2 Phase transition and state switching

There are two types of phase transitions involved in boiling: the vaporization of liquid into vapor and the condensation of vapor into liquid. Vaporization occurs when the liquid temperature reaches the saturation temperature and nucleation sites are present to facilitate vaporization. In contrast, condensation, which is the reverse process of evaporation, occurs when the temperature of the vapor falls below the saturation temperature.

The phase transition of liquid particles requires two conditions to be simultaneously satisfied: a thermodynamic condition, which requires the temperature to rise to the phase transition temperature T_{phase}, and a kinetic condition, which necessitates the presence of nucleation sites in the vicinity. Due to the effects of heat conduction and convection, the liquid undergoes various complex phenomena that cause instantaneous switching between the two phase transition conditions. This results in interruptions and resumptions of particle phase transitions, thereby inducing conversions between the latent and sensible heat.

For instance, when liquid particles accumulate latent heat during a phase transition near nucleation sites, heat convection may carry them away from these regions, thereby interrupting the phase transition process. Consequently, the heat absorbed by these particles through conduction or convection no longer contributes to latent heat accumulation but instead increases the sensible heat, resulting in temperature changes. Conversely, when superheated particles are transported by convective flows back toward nucleation sites, they meet the phase transition conditions and resume a phase transition. In this case, the superheated portion of the sensible heat is converted into latent heat, and subsequently, absorbed heat continues to accumulate as latent heat.

To facilitate the handling of instantaneous sensible-to-latent heat conversions caused by particle state transitions, we classify particles into four distinct states: normal liquid, undergoing phase transition, superheated liquid, and vapor. Among them, normal liquid refers to liquid particles with temperatures below the saturation temperature; undergoing phase transition represents particles currently undergoing phase change; superheated liquid denotes liquid particles in the superheated state; and vapor corresponds to gaseous particles.

Specifically, we decide per state whether heat transfer is latent or sensible, shown in Table 1. Since only particles in the undergoing phase change state exchange heat in the form of latent heat, while all other states involve sensible heat transfer, it is necessary to define the transition conditions between the undergoing phase change state and the other states, as well as the corresponding update rules, shown in Figure 2. The aforementioned cases of phase transition interruption and recovery correspond to two types of state transitions that alter the kinetic condition. Phase transition interruption, causes the kinetic condition to become unsatisfied, corresponding to the transition from undergoing phase change to superheated liquid in Figure 2. In this case, the latent heat currently stored is converted into sensible heat, and the mode of heat transfer switches from latent to sensible. Conversely, phase transition recovery, causes the kinetic condition to become satisfied again, corresponding to the transition from superheated liquid to undergoing

phase change in Figure 2. In this case, the sensible heat exceeding the saturation temperature is converted into latent heat, and the heat transfer mode switches from sensible to latent.

Particle State	Type of Heat Transfer
Normal liquid	Sensible heat
Undergoing phase transition	Latent heat
Superheated liquid	Sensible heat
Vapor	Sensible heat

Table 2: Classification of heat transfer types for different particle states.

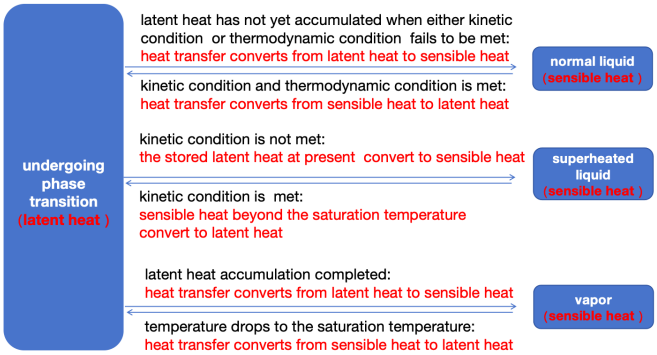

Figure 2: State transition diagram showing the triggering conditions and the corresponding changes in heat transfer type.

4. Bubble simulation

4.1. Connected vapor particle detection

To identify connected vapor particle clusters, we adopt a parallel union–find (disjoint set) algorithm. Each vapor particle is initially assigned a unique parent label corresponding to its index. For every pair of neighboring vapor particles, a union operation is performed to merge their sets if they are within the interaction radius. During the union process, path compression and union-by-rank strategies are applied to minimize the depth of the disjoint-set trees and accelerate convergence. After all union operations are completed, the root label of each particle is determined using the find operation. Vapor particles sharing the same root label are then identified as belonging to the same bubble, with the root label serving as the unique identifier for that bubble. This approach efficiently detects connectivity among vapor particles with near-linear time complexity and is well suited for parallel implementation on modern computing architectures.

4.2. Bubble behavior

By identifying vapor particles with the same label, we determine the number of particles num_p contained in each bubble, which correlates with the bubble's volume. According to Archimedes' principle, a consistent buoyancy force is applied to all particles within the same bubble:

$$\mathbf{F}_{\text{buoyancy}} = \rho_{liquid} \cdot V_{bubble} \cdot \mathbf{g}, \tag{18}$$

where ρ_{liquid} is the density of the surrounding liquid, V_{bubble} is the bubble volume. Using the relation $V_{bubble} = k_{bubble} \cdot num_p$, where k_{bubble} is a proportionality constant, num_p denotes the number of vapor particles sharing the same label, i.e., the total number of particles belonging to the same bubble. We derive the following expression:

$$\mathbf{F}_{\text{buoyancy}} = k_{bubble} \cdot \rho_{liquid} \cdot num_p \cdot \mathbf{g}. \tag{19}$$

This ensures velocity coherence among particles within the bubble, preventing excessive velocity divergence that could otherwise lead to premature bubble fragmentation.

The lifecycle of a bubble is of fundamental importance in our simulation. It begins when a liquid particle transitions into the vapor phase. This will be discussed in more detail below.

4.2.1 Bubble expansion and detachment

A bubble grows as vapor particles accumulate, leading to an increase in both the volume and buoyancy. Once the buoyant force overcomes both the surface tension and resistance, the bubble detaches and rises.

4.2.2 Bubble condensation

During the ascent, bubbles may undergo condensation due to heat transfer. We track the thermal energy losses of all the vapor particles that are in the process of phase transition, specifically those whose temperatures decrease to the saturation temperature. The total thermal energy consumed during condensation is calculated as

$$Q_{\text{cond},b} = \sum_{i \in b, T_i < T_{\text{sat}}} m_i c \left(T_{\text{sat}} - T_i\right), \tag{20}$$

where $Q_{\text{cond},b}$ denotes the total thermal energy consumed during condensation of bubble b, i denotes one of the vapor particles within bubble b that satisfies $T_i < T_{sat}$. The total thermal energy consumed results in the phase transition of n vapor particles into the liquid state:

$$n = \lfloor Q_{\text{cond},b} / L \rfloor. \tag{21}$$

The Fisher–Yates shuffle algorithm is used to randomly select n particles to undergo a phase transition, with the residual energy defined as follows:

$$Q_{residual} = Q_{\text{cond},b} - n \cdot L. \tag{22}$$

The residual thermal energy is insufficient for a phase transition and is consequently redistributed among the remaining $k - n$ particles.

After the phase transition, the number of particles num_p within the bubble decreases, causing the bubble to shrink. Eventually, the bubble either condenses back into the liquid or breaks through the liquid surface.

4.3. Bubble oscillation constraint

We observed that during the actual rising and merging processes, bubbles exhibit periodic expansion and contraction, with their volumes undergoing distinct cycles of shrinking and expanding, as shown in Figures 7 and 8. Therefore, we developed an empirical bubble oscillation constraint based on the number of vapor particles within each bubble, the average bubble radius, and the experimentally observed range of average bubble radius.

Since the number of vapor particles N within a bubble is proportional to the bubble volume, and the bubble volume is proportional to R^3, the average bubble radius R is therefore proportional to $N^{1/3}$. Based on our experimental observations, the most realistic oscillation behavior is achieved when the bubble begins to expand once its average radius falls below $r_{\min}(N) = 0.45 + k_{model}N^{1/3}$, and begins to contract once it exceeds $r_{\max}(N) = 0.85 + k_{model}N^{1/3}$, where $k_{model} = 0.05$ is an adjustment coefficient. The detailed implementation of this model is described below.

First, for each bubble, we compute the average position of its vapor particles as follows:

$$\mathbf{p}_{\text{avg}} = \frac{1}{N}\sum_{i\in b}\mathbf{p}_i, \tag{23}$$

where $\mathbf{p}_i$ is the position of the i-th particle, b denotes the set of all vapor particles contained within the bubble. We also calculated the average radius of vapor particles within each bubble, as follows:

$$r_{\text{avg}} = \frac{1}{N}\sum_{i}\|\mathbf{x}_i - \mathbf{P}_{\text{avg}}\| \tag{24}$$

Two unilateral constraints are defined to enforce the above bounds:

$$\begin{aligned} C_{\text{expand}}(b) &= r_{\min}(N) - r_{\text{avg}} \le 0, \\ C_{\text{shrink}}(b) &= r_{\text{avg}} - r_{\max}(N) \le 0. \end{aligned} \tag{25}$$

Only the violated constraint ($C > 0$) is solved during each iteration. For example, when r_{avg} is less than $r_{min}(N)$, $C_{\text{expand}}(b)$ will be solved.

The gradient of the constraint is computed as follows:

$$\begin{aligned} \nabla_{x_i} C_{\text{expand}}(b) &= -\nabla_{x_i} r_{\text{avg}}, \\ \nabla_{x_i} C_{\text{shrink}}(b) &= \nabla_{x_i} r_{\text{avg}}, \end{aligned} \tag{26}$$

where ∇r_{avg} is the gradient of the average bubble radius with respect to particle positions, indicating how the mean radius changes when a particle moves, which is computed from Equation (24):

$$\nabla_{x_i} r_{\text{avg}} = \frac{1}{N}\frac{\mathbf{x}_i - \mathbf{P}_{\text{avg}}}{\|\mathbf{x}_i - \mathbf{P}_{\text{avg}}\|} - \frac{1}{N^2}\sum_{j=1}^{N}\frac{\mathbf{x}_j - \mathbf{P}_{\text{avg}}}{\|\mathbf{x}_j - \mathbf{P}_{\text{avg}}\|}. \tag{27}$$

The second term arises from the dependence of P_{avg} on each particle position x_i. This term numerically cancels out, as the directional vectors from all particles toward the bubble center approximately sum to zero on average. For numerical simplicity, we approximate the gradient of the average radius with respect to each particle as:

$$\nabla_{\mathbf{x}_i} r_{avg} \approx \frac{1}{N}\frac{\mathbf{x}_i - \mathbf{P}_{\text{avg}}}{\|\mathbf{x}_i - \mathbf{P}_{\text{avg}}\| + \epsilon} = \frac{\mathbf{d_i}}{N}, \tag{28}$$

where $\mathbf{d_i}$ is the normalized direction vector from the bubble center to the particle, and ϵ is a small regularization term to avoid division by zero.

For each violated constraint $C \in \{C_{\text{expand}}(b), C_{\text{shrink}}(b)\}$ we compute the Lagrange multiplier:

$$\lambda = -\frac{C}{\sum_{i\in b} w_i\|\nabla C\|^2 + \varepsilon}, \tag{29}$$

where w_i is the inverse mass of particle i and ε is a small stabilization constant.

The position correction for each particle is then:

$$\Delta\mathbf{x}_i = \omega w_i \lambda \nabla_{\mathbf{x}_i} C \tag{30}$$

where $\omega \in (0, 1]$ is an under-relaxation coefficient used to suppress high-frequency oscillations.

Therefore, when $C_{\text{expand}}(b) > 0$, the gradient $\nabla C_{\text{expand}}(b)$ is negative, causing the particles to move outward; when $C_{\text{shrink}}(b) > 0$, the gradient $\nabla C_{\text{shrink}}(b)$ is positive, resulting in particles moving inward. Bubble oscillation constraint is an empirical model designed to adjust particle positions in a controlled manner to achieve visually realistic results.

The empirical constants involved in the bubble oscillation constraint and dynamic nucleation are summarized in Table 3. We evaluated the sensitivity of these parameters by perturbing them within reasonable ranges. The results indicate that the oscillation bounds $r_{\min}(N)$ and $r_{\max}(N)$ mainly regulate the amplitude range of bubble oscillation, while the oscillation coefficient k_{model} influences the response intensity of the oscillatory behavior. The under-relaxation coefficient ω primarily affects numerical stability and convergence. Overall, the proposed oscillation model exhibits low sensitivity to these empirical constants, and small variations do not alter the qualitative oscillation behavior.

Table 3: Parameters for bubble oscillation and dynamic nucleation.

	Description	Default Value	Sensitivity
$r_{\min}(N)$	Minimum oscillation radius	$0.45 + 0.05N^{1/3}$	Low sensitivity; mainly affects oscillation lower bound.
$r_{\max}(N)$	Maximum oscillation radius	$0.85 + 0.05N^{1/3}$	Low sensitivity; controls oscillation upper bound.
k_{model}	Oscillation coefficient	0.05	Moderate sensitivity; influences oscillation intensity.
Q_{crit}	Dynamic nucleation threshold	$10m_pL$	Moderate sensitivity; higher values suppress explosive boiling, lower values trigger it more often.

5. Algorithm

Our simulation loop is summarized in Algorithm 1. The boiling simulation is conducted within the PBF framework. Lines 1–4 compute heat transfer and temperature gradients, corresponding to Section 3.3.1. Lines5-7 handle bubble condensation. Lines 8-11 handle phase transition processes for preset and dynamic nucleation sites, corresponding to Sections 3.2, 3.3.3, and 4.2.2. After phase transition, lines 12–14 perform connectivity analysis of vapor particles to identify individual bubbles, as described in Section 4.1. Lines 15–20 then compute the total forces, predict the next-frame positions, and conduct neighbor searches, corresponding to Section 4.2. Lines 21–26 apply the PBF density constraint to correct the predicted positions, as explained in Section 3.1. Subsequently, lines 27–35 enforce the bubble oscillation constraint on the corrected positions, corresponding to Section 4.3. Finally, lines 36–39 update particle velocities and positions based on the corrected positions and those from the previous frame.

6. Results

In this section, we demonstrate the results of our proposed method in various simulated scenes. First, we present the overall simulation results throughout the boiling process, validating its ability to capture complex bubble dynamics. Subsequently, we construct a test scenario where the heat source is removed to demonstrate boiling heat transfer during the cooling phase. In addition, we investigate the role of dynamic nucleation during bubble formation, as well as the effects of the bubble oscillation constraint on bubble rising, merging, and splitting. To systematically reveal the contribution of each mechanism, we conduct ablation studies by disabling dynamic nucleation or removing the oscillation constraint, and compare the resulting behaviors to highlight their importance. Finally, we evaluate the stability and robustness of the proposed framework under different simulation conditions, using both quantitative and qualitative results to demonstrate its effectiveness.

Algorithm 1 Simulation Loop

1: **for** all particle **do**
2: heat conduction and convection calculations
3: temperature gradient calculation
4: **end for**
5: **for** all vapor particle **do**
6: condensation detection
7: **end for**
8: **for** all liquid particle **do**
9: preset nucleation sites phase transition
10: dynamic nucleation detection
11: **end for**
12: **for** all vapor particle **do**
13: find connected particles
14: **end for**
15: **for** all particle **do**
16: save old particle information $\mathbf{v_i}$ and $\mathbf{x_i}$
17: apply force $\mathbf{v_i^*} \leftarrow \mathbf{v_i} + \Delta t \mathbf{f_{ext}}(\mathbf{x_i})$
18: predict position $\mathbf{x_i^*} \leftarrow \mathbf{x_i} + \Delta t \mathbf{v_i}$
19: find neighboring particles
20: **end for**
21: **while** $iter < solverIterations$ **do**
22: **for** all particle **do**
23: solve all density constraints for $\Delta\mathbf{x}$
24: update position $\mathbf{x_i^*} \leftarrow \mathbf{x_i^*} + \omega\Delta\mathbf{x}$
25: **end for**
26: **end while**
27: **while** $iter < n_{steps}$ **do**
28: **for** all vapor particle **do**
29: Evaluate average radius r_{avg} and thresholds r_{min}, r_{max}
30: **if** $r_{avg} < r_{min}$ or $r_{avg} > r_{max}$ **then**
31: Solve bubble constraint for all particles in b
32: Update positions: $\mathbf{x}_i^* \leftarrow \mathbf{x}_i^* + \omega\, w_i\, \lambda\, \nabla_{\mathbf{x}_i} C$
33: **end if**
34: **end for**
35: **end while**
36: **for** all particles **do**
37: update velocity $\mathbf{v_i} \leftarrow \frac{1}{\Delta t}(\mathbf{x_i^*} - \mathbf{x_i})$
38: update position $\mathbf{x_i} \leftarrow \mathbf{x_i^*}$
39: **end for**

All examples are run on a laptop with a 6-core 2.6GHz CPU, an NVIDIA GeForce RTX 2060 graphics card and 16 GB of RAM. The simulation results were compared with results from experiments in which water was heated from the bottom in a transparent vessel under ambient pressure at room temperature. The heat source provided a constant input to the liquid, allowing bubble nucleation and growth. The vessel allowed clear observation of the boiling process, and images were captured from a frontal view to track the bubble dynamics, such as rising, merging, and detachment.

Figure 3 compares our simulated steady boiling with real experimental observations. Our results exhibit realistic bubble rising behavior. We attribute this behavior to the bubble oscillation constraint, which causes each bubble to undergo periodic expansion and contraction during ascent, producing pulsation patterns that are closer to those observed in experiments than in previous methods.

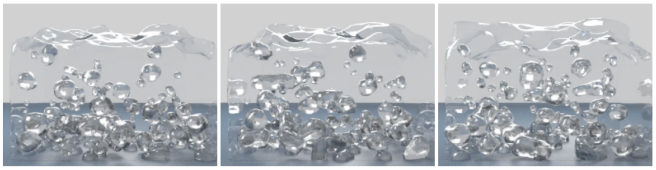

(a) Our simulation

(b) Actual boiling

Figure 3: Comparison between our boiling simulation and actual boiling

After the external heat source is removed, our model continues to simulate bubble condensation and restabilization of the liquid–vapor interface. The comparison in Figure 4 demonstrates that the model captures the gradual disappearance of vapor regions and reproduces realistic cooling dynamics, which were rarely addressed in previous works.

Previous particle-based boiling simulation methods often fail to accurately capture explosive boiling phenomena, primarily due to their neglect of the kinetic condition of phase transition and the absence of an effective protection mechanism for superheated liquid particles. In contrast, we propose a dynamic nucleation mechanism inspired by classical nucleation theory (CNT). By monitoring the local thermal energy distribution, temporary cavities are spontaneously formed when the temperature or energy in a superheated region exceeds a critical threshold. These cavities are treated as transient vapor nuclei, initiating large-scale phase transitions and significantly improving the thermal stability of the system. As shown by the red box in Figure 5, this mechanism enables spontaneous and explosive bubble formation, which is essential for accurately reproducing explosive boiling and is absent in prior particle-based methods.

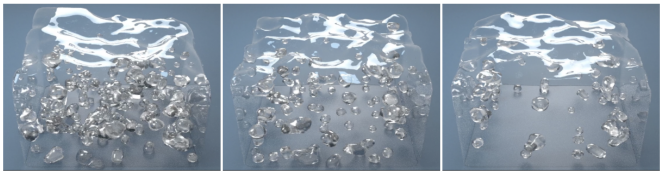

(a) Our simulation

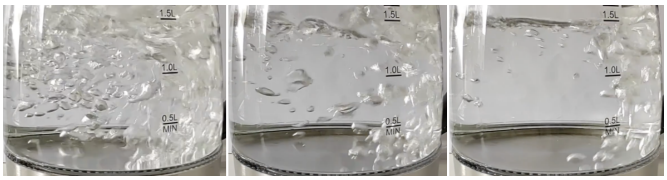

(b) Actual boiling

Figure 4: Comparison between our simulation results and actual boiling after heating was stopped

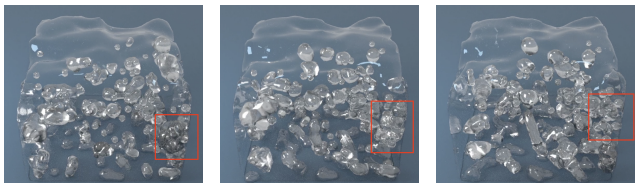

(a) (b) (c)

Figure 5: Explosive boiling

To further validate the independent contribution of the dynamic nucleation mechanism, we design an ablation experiment in which the bubble oscillation constraint is removed while the dynamic nucleation mechanism is retained. This simplified setup isolates the effect of dynamic nucleation alone. As shown in Figure 6, despite the absence of oscillation-based regulation on bubble morphology, the system is still able to achieve continuous and spontaneous bubble nucleation in superheated regions, converting a large amount of excess sensible heat into latent heat. This result demonstrates that the dynamic nucleation mechanism itself has a strong capability to drive bubble generation, as well as significant potential for restoring thermal stability.

Figure 7 shows the comparison between our simulation

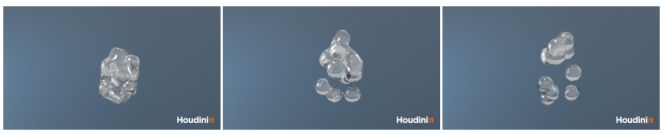

Figure 6: Ablation Study of the Dynamic Nucleation Mechanism

results and actual rising bubbles. In the figure, red boxes highlight a specific bubble to illustrate its rising process, allowing visual comparison of the bubble's shape, trajectory, and behavior between the simulation and experiment. Figure 8 shows the comparison between our simulation results and actual merging bubbles. Figure 9 shows the comparison between our simulation results and actual splitting bubbles.

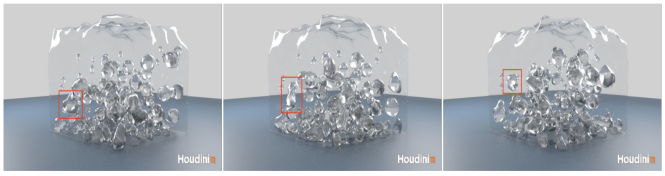

(a) Our simulation

(b) Actual boiling

Figure 7: Comparison between our simulation results and actual rising bubbles

To further validate the independent role of the oscillation constraint, we design an ablation experiment in which the dynamic nucleation mechanism is removed while the bubble oscillation constraint is retained, resulting in a simplified scenario with oscillation effects only. Figure 10 illustrates the bubble rising process, Figure 11 shows bubble merging, and Figure 12 depicts bubble splitting. Although the system lacks the bubble generation capability and explosive boiling behavior provided by dynamic nucleation, it is still able to realistically reproduce the morphological evolution and motion of bubbles during rising, merging, and splitting. These results confirm the important role of the oscillation constraint in producing visually plausible bubble dynamics.

We compare the proposed method with previous approaches in terms of boiling behavior, as shown in Figure 13. In Gu et al. [8], a liquid particle enters the phase-

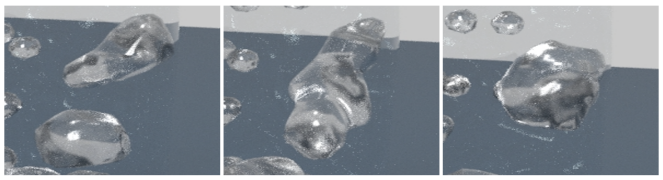

(a) Our simulation

(b) Actual boiling

Figure 8: Comparison between our simulation results and actual merging bubbles

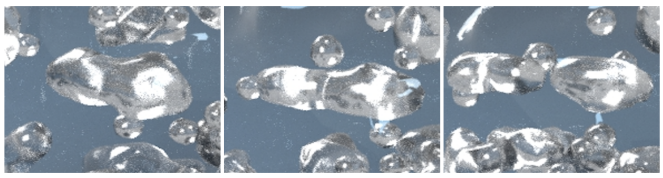

(a) Our simulation

(b) Actual boiling

Figure 9: Comparison between our simulation results and actual splitting bubbles

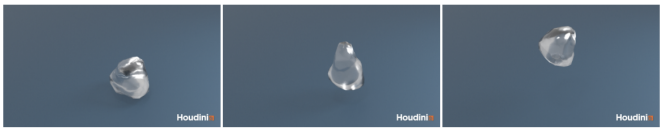

Figure 10: Ablation experiment of bubble oscillation constraint: bubble rise

transition process immediately after satisfying the thermodynamic condition. Since the kinetic conditions of phase change are not considered, the method is incapable of modeling superheating. A detailed comparison of the number of superheated particles produced by each method is presented

Figure 11: Ablation experiment of bubble oscillation constraint: bubble merge

Figure 12: Ablation experiment of bubble oscillation constraint: bubble split

in Figure 14. Li et al. [12] allows the formation of superheated liquid since they focus solely on nucleation sites, without considering the thermodynamic or kinetic conditions of individual liquid particles. Although a single nucleation site could generate multiple bubbles over time, only one bubble could originate from the same site at any given moment, thereby the total number of bubbles is inherently limited by the number of predefined nucleation sites. Moreover, this method does not model a mechanism for releasing excess energy stored in superheated liquids, causing superheating to instead undermine the stability of the system.

The proposed approach enables the formation of superheated liquid by ensuring that both thermodynamic and kinetic criteria are simultaneously satisfied at the particle level. In addition, a thermally induced dynamic nucleation mechanism is incorporated to regulate energy buildup. When a liquid particle's sensible heat surpasses a specified threshold, temporary microscopic cavities are generated, satisfying the kinetic conditions for phase transition, thereby triggering the phase change and restoring local energy to a stable state. Through this thermally driven dynamic nucleation mechanism, our method not only reproduces the formation of superheated liquids but also provides a protection mechanism for the superheated metastable state. By avoiding reliance on fixed, predefined nucleation sites, the proposed approach more faithfully captures the energy exchange and phase transition kinetics between liquid and gas during boiling. Compared with previous methods, our approach significantly enhances the capability of particle-based boiling simulations, accurately reproducing superheated liquids while maintaining system stability through dynamic nucleation.

To assess the computational efficiency of the proposed method, performance was measured across multiple simulation scenarios, including explosive boiling, steady nucleate boiling, post-heating cooling, and bubble rising, merging, and splitting. The performance statistics, including particle

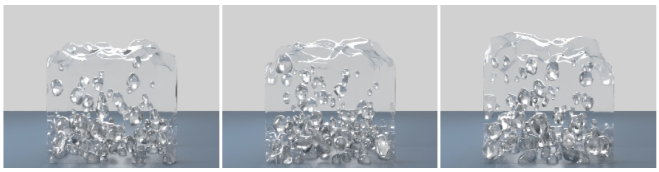

(a) Boiling simulation results of our method

(b) Boiling simulation results of Gu et al. [8]

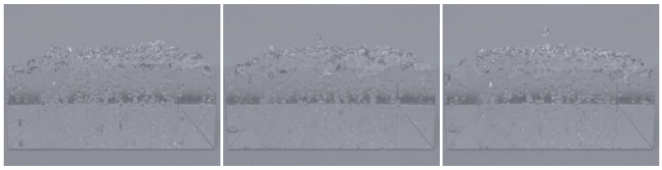

(c) Boiling simulation results of Li et al. [12]

Figure 13: Comparison between our boiling simulation and previous boiling simulation

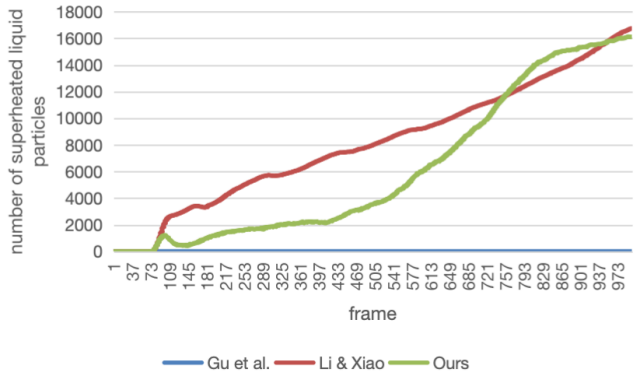

Figure 14: Comparison of superheated particles

counts and average frame rates, are summarized in Table 3.

Finally, we further evaluate the proposed method using the temporal evolution of the average bubble radius, as shown in Fig. 15. The curve exhibits a clear transient peak at the early stage, followed by a gradual relaxation and a stable regime. This trend is consistent with boiling dynamics observed in real-world phenomena, where bubble growth is initially accelerated by local superheating and then stabilizes due to heat depletion and the continuous interaction

Table 4: Performance summary of the proposed boiling simulation under different scenarios.

Scenario	Figure	Particle Count	Avg. FPS	Key Observations
Steady boiling	Fig. 3	20k	22.7	Consistent bubble generation and stable nucleation cycles.
Post-heating cooling	Fig. 4	20k	25.2	Gradual condensation and smooth vapor–liquid transition.
Explosive boiling	Fig. 5	20k	24.4	Realistic explosive onset and rapid bubble nucleation.
Bubble rising	Fig. 7	20k	23.3	Bubble trajectories and shapes closely match experiments.
Bubble merging	Fig. 8	20k	22.9	Correct surface tension and coalescence dynamics.
Bubble splitting	Fig. 9	20k	23.4	Physically plausible breakup and volume conservation.

with surrounding flow. Overall, the curve indicates that the proposed model produces plausible bubble-scale behavior.

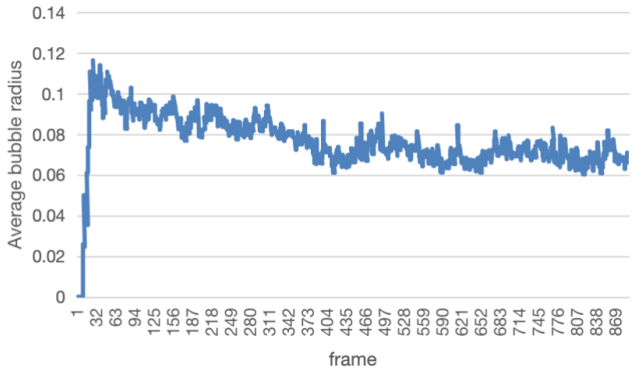

Figure 15: Transition of Average Bubble Radius During Boiling Process

7. Conclusions

In this paper, the proposed method overcomes a major limitation of boiling simulations by explicitly incorporating the kinetic conditions of phase transition, enabling realistic modeling of superheating phenomena. To avoid unphysical energy buildup in superheated regions, a thermally induced dynamic nucleation mechanism inspired by classical nucleation theory is introduced. When the local sensible heat exceeds a critical value, a temporary microscopic cavity is formed, acting as a transient nucleation site. This allows nearby superheated liquid to fulfill the kinetic criterion for phase transition. The excess sensible heat is subsequently converted into latent heat, restoring local thermal balance and maintaining system stability. This mechanism effectively reproduces the metastable superheating state observed in real boiling and enhances both the physical accuracy and numerical robustness of the simulation.

While the dynamic nucleation mechanism ensures correct initiation of phase change in superheated regions, accurate simulation also requires proper accounting of energy transfer. To this end, we propose a novel dual-channel phase transition model that distinctly separates the roles of sensible and latent heat. A liquid phase transition requires both thermodynamic conditions (reaching a critical temperature) and kinetic conditions (the presence of nucleation sites). Due to heat conduction and convection effects, phase transition conditions may switch instantaneously. For example, convective flow can interrupt the phase transition by transporting transitioning particles away from nucleation sites or restore the phase transition by delivering superheated particles to regions with available nucleation sites. These dynamic scenarios result in switching between sensible and latent heat treatments. To address this, we classify particles into four states: normal liquid, undergoing phase transition, superheated liquid, and vapor. This classification ensures that sensible and latent heat treatments are dynamically adjusted in response to changes in the kinetic or thermodynamic conditions, maintaining energy conservation and accurate energy conversion.

It was observed that during ascent, bubbles underwent periodic contraction and expansion, with their volumes following distinct oscillatory cycles. To replicate this phenomenon, connected vapor particles were identified and grouped as individual bubbles. A bubble oscillation constraint was then applied to each bubble, allowing periodic variation in its volume and shape. This constraint enabled cyclic fluctuations in bubble geometry, thereby enhancing the physical realism of the simulation.

Finally, we observed that during the early stages of boiling, bubbles rapidly condensed while rising, accompanied by cavitation effects. Specifically, bubbles ruptured and were pierced by micro-jets into ring-like structures, which subsequently broke down into multiple smaller bubbles. This remains a highly challenging phenomenon to simulate accurately. In addition, the current bubble oscillation constraint is implemented empirically to reproduce realistic pulsation, and a potential future work direction is to replace it with a physically-based bubble dynamics model.

Acknowledgement

This work was supported by the National Natural Science Foundation of China (62272305) and the National Key Research and Development Program of China (2018YFB1004902).

References

[1] J. Bender and D. Koschier. Divergence-free sph for incompressible and viscous fluids. *IEEE Transactions on Visualization and Computer Graphics*, 23(3):1193–1206, 2016. 3

[2] A. Bulbul, O. Kucuktunc, and B. Ozguc. Animation of boiling phenomena. In *2008 3DTV Conference: The True Vision-Capture, Transmission and Display of 3D Video*, pages 357–360, New York, NY, USA, 2008. IEEE. 3

[3] M. Carlson, P. J. Mucha, R. B. Van Horn III, and G. Turk. Melting and flowing. In *Proceedings of the 2002 ACM SIGGRAPH/Eurographics symposium on Computer animation*, pages 167–174, New York, NY, USA, 2002. Association for Computing Machinery. 3

[4] W. Chen, T. Sang, Y. Ma, Q. Chen, Y. Xiao, Z. Pan, and X. Yang. Real-time simulation of violent boiling in concentrated sulfuric acid dilution. *The Visual Computer*, 37(9–11):2631–2642, 2021. 3

[5] P. Clausen, M. Wicke, J. R. Shewchuk, and J. F. O'brien. Simulating liquids and solid-liquid interactions with lagrangian meshes. *ACM Transactions on Graphics (TOG)*, 32(2):1–15, 2013. 3

[6] M. Ding, X. Han, S. Wang, T. F. Gast, and J. M. Teran. A thermomechanical material point method for baking and cooking. *ACM Transactions on Graphics (TOG)*, 38(6):1–14, 2019. 3

[7] M. Gao, X. Wang, K. Wu, A. Pradhana, E. Sifakis, C. Yuksel, and C. Jiang. Gpu optimization of material point methods. *ACM Transactions on Graphics (TOG)*, 37(6):1–12, 2018. 3

[8] Y. Gu and Y.-H. Yang. Physics based boiling bubble simulation. In *SIGGRAPH ASIA 2016 Technical Briefs*, New York, NY, USA, 2016. Association for Computing Machinery. 2, 3, 6, 11, 12

[9] M. Ihmsen, J. Cornelis, B. Solenthaler, C. Horvath, and M. Teschner. Implicit incompressible sph. *IEEE Transactions on Visualization and Computer Graphics*, 20(3):426–435, 2013. 3

[10] K. Iwasaki, H. Uchida, Y. Dobashi, and T. Nishita. Fast particle-based visual simulation of ice melting. In *Computer graphics forum*, volume 29, pages 2215–2223, Hoboken, New Jersey, U.S., 2010. Wiley Online Library. 3

[11] T. Kim and M. Carlson. A simple boiling module. In *Proceedings of the 2007 ACM SIGGRAPH/Eurographics symposium on Computer animation*, pages 27–34, Goslar, DEU, 2007. Eurographics Association. 3

[12] Z. Li and S. Xiao. Boiling simulation of position based fluid. In *Proceedings of the 4th International Conference on Virtual Reality*, pages 142–146, New York, NY, USA, 2018. Association for Computing Machinery. 1, 2, 3, 12

[13] Y. Liu, T. Zhang, X. Yan, N. Liu, and B. Ren. Controllable complex freezing dynamics simulation on thin films. *ACM Transactions on Graphics (TOG)*, 44(4):1–12, 2025. 3

[14] L. B. Lucy. A numerical approach to the testing of the fission hypothesis. *The Astronomical Journal*, 82(12):1013–1024, 1977. 2

[15] M. Macklin and M. Müller. Position based fluids. *ACM Transactions on Graphics (TOG)*, 32(4):1–12, 2013. 1, 3

[16] V. Mihalef, B. Unlusu, D. Metaxas, M. Sussman, and M. Y. Hussaini. Physics based boiling simulation. In *Proceedings of the 2006 ACM SIGGRAPH/Eurographics symposium on Computer animation*, pages 317–324, Goslar, DEU, 2006. Eurographics Association. 3

[17] M. Müller, D. Charypar, and M. Gross. Particle-based fluid simulation for interactive applications. In *Proceedings of the 2003 ACM SIGGRAPH/Eurographics symposium on Computer animation*, pages 154–159, Goslar, DEU, 2003. Eurographics Association. 2

[18] M. Müller, B. Heidelberger, M. Hennix, and J. Ratcliff. Position based dynamics. *Journal of Visual Communication and Image Representation*, 18(2):109–118, 2007. 1, 3

[19] M. Prakash, P. W. Cleary, S. H. Pyo, and F. Woolard. A new approach to boiling simulation using a discrete particle based method. *Computers & Graphics*, 53:118–126, 2015. 2, 3

[20] B. Solenthaler and R. Pajarola. Predictive-corrective incompressible SPH. In *ACM SIGGRAPH 2009 Papers*, pages 1–6, New York, NY, USA, 2009. Association for Computing Machinery. 3

[21] A. D. Stojanović, S. V. Belošević, N. . Crnomarković, I. D. Tomanović, and A. R. Milićević. Nucleate pool boiling heat transfer: Review of models and bubble dynamics parameters. *Thermal Science*, 26(1 Part A):157–174, 2022. 2

[22] A. Stomakhin, C. Schroeder, C. Jiang, L. Chai, J. Teran, and A. Selle. Augmented mpm for phase-change and varied materials. *ACM Transactions on Graphics (TOG)*, 33(4):1–11, 2014. 3

[23] D. Stora, P.-O. Agliati, M.-P. Cani, F. Neyret, and J.-D. Gascuel. Animating lava flows. In *Proceedings of the 1999 Conference on Graphics Interface '99*, pages 203–210, San Francisco, CA, USA, 1999. Morgan Kaufmann Publishers Inc. 3

[24] H. Su, T. Xue, C. Han, C. Jiang, and M. Aanjaneya. A unified second-order accurate in time mpm formulation for simulating viscoelastic liquids with phase change. *ACM Transactions on Graphics (TOG)*, 40(4):1–18, 2021. 3

[25] Z. Tu, C. Li, Z. Zhao, L. Liu, C. Wang, C. Wang, and H. Qin. A unified mpm framework supporting phase-field models and elastic-viscoplastic phase transition. *ACM Transactions on Graphics (TOG)*, 43(2):1–19, 2024. 3